Matter

CellPress

Article

Morphing of stiffness-heterogeneous liquid crystal elastomers via mechanical training and locally controlled photopolymerization

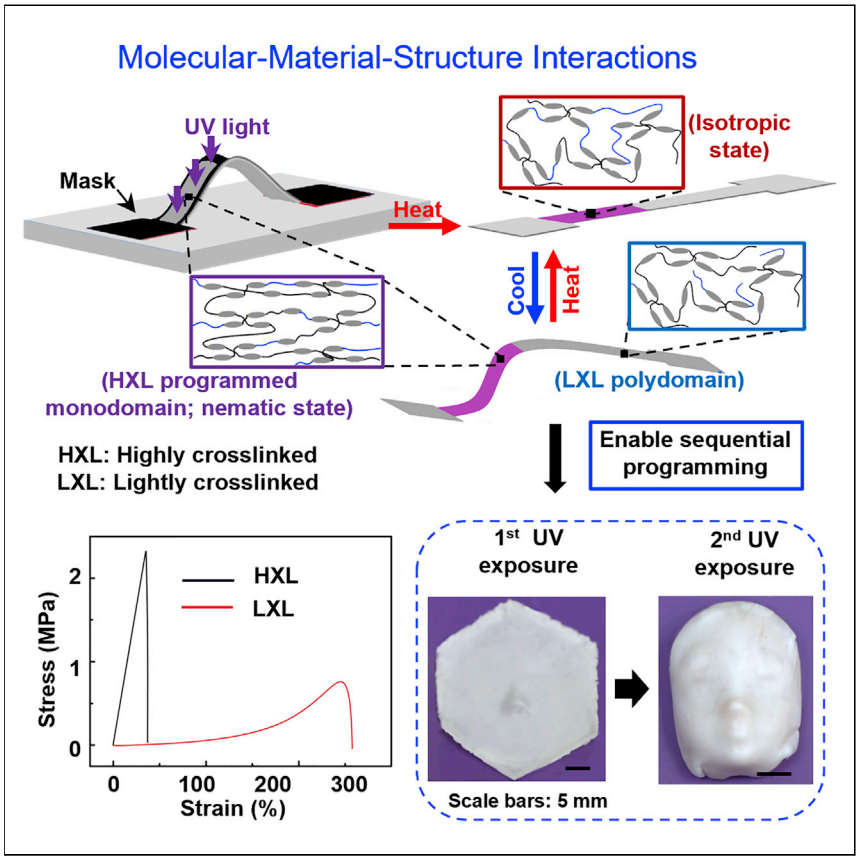

Tailoring the local stiffness and morphing behaviors of reconfigurable structures would create new opportunities for many applications, including in soft robotics, but is usually challenging to achieve. Herein, we present a facile strategy to harness the molecular-material-structural interactions of liquid crystal elastomers to create diverse stiffness-heterogeneous, reversibly morphing structures via locally controlled photopolymerization and mechanical training. Sequential programming of non-photopolymerized regions allows for reshaping of the programmed structures, like in a "face" that can sequentially display facial features.

Demonstrate
Proof-of-concept of performance with intended application/response

Yi Li, Gina Parlato, Francis K. Masese, Rajeswari M. Kasi, Teng Zhang, Xueju Wang

tzhang48@syr.edu (T.Z.)
xueju.wang@uconn.edu (X.W.)

Highlights

Facile strategy to tailor the stiffness and morphing of liquid crystal elastomers

Selective molecular crosslinking and alignment via light and mechanical programming

Creation of various asymmetric, stiffness-heterogeneous shape-morphing structures

Sequential programming of non-photopolymerized regions for reshaping of structures

Li et al., Matter 5, 1–15
December 7, 2022
https://doi.org/10.1016/j.matt.2022.08.019

Please cite this article in press as: Li et al., Morphing of stiffness-heterogeneous liquid crystal elastomers via mechanical training and locally controlled photopolymerization, Matter (2022), https://doi.org/10.1016/j.matt.2022.08.019

Matter

CellPress

Article

Morphing of stiffness-heterogeneous liquid crystal elastomers via mechanical training and locally controlled photopolymerization

Yi Li,[1] Gina Parlato,[1] Francis K. Masese,[2] Rajeswari M. Kasi,[2,3] Teng Zhang,[4,5,*] and Xueju Wang[1,3,6,*]

SUMMARY

The large, reversible shape-changing behaviors of liquid crystal elastomers (LCEs), resulting from liquid crystal-polymer network couplings, are promising for many applications. Despite intensive studies, harnessing molecular-material-structure interactions of LCEs for the design of locally controlled shape-morphing structures remains a challenge. Here, we report a facile and versatile strategy to tailor the stiffness and the morphing behavior of reconfigurable LCE structures via locally controlled mesogen alignment and crosslinking densities. Selective photopolymerization of spatially aligned LCE structures yields well-controlled lightly and highly crosslinked domains of distinct stiffness and selective permanent mesogen programming, which enables various previously inaccessible stiffness-heterogeneous geometries, as demonstrated in diverse morphing LCE structures via integrated experimental and finite element analysis. Furthermore, programming of the non-photopolymerized regions allows for reshaping, as shown in a sequentially shape-morphing LCE rod and "face". The heterogenous morphing LCE structures have the potential for many applications, including in artificial muscles, soft robotics, and many others.

PROGRESS AND POTENTIAL

Adaptive structures of stimuli-responsive materials that can change their shapes and therefore functionalities are promising for many applications including soft robotics and biomedical devices. Capabilities for the local control of their material properties and morphing behaviors have been desired but remain a challenge. Here, we introduce a facile technique to create stiffness-heterogeneous morphing structures of liquid crystal elastomers via selective photopolymerization and mechanical programming. More specifically, tailoring molecular interactions enables material regions of distinct stiffness, which synergistically determines the morphing behavior of diverse asymmetric three-dimensional structures and subsequent sequential programming of the structure. The results represent a significant step toward creating next-generation intelligent materials and structures with well-controlled properties for engineering applications.

INTRODUCTION

Structures composed of soft, stimuli-responsive materials including hydrogels,[1,2] shape memory polymers,[3–6] dielectric elastomers,[7,8] magnetically responsive composites,[9–12] and liquid crystal elastomers (LCEs),[13–19] are of growing interest for many potential applications such as biomedical devices,[20–22] deployable solar panels,[23,24] soft robotics,[9,25] and many others. Such structures can respond to external stimuli (e.g., light, electric field, magnetic field, pH, temperature, and pressure) to achieve targeted reconfigurations. Recently, LCEs, which combine the rubber elasticity of polymer networks with the orientational order of liquid crystals (LCs, mesogens),[13–16,25–36] have received much attention for their unique properties, including soft elasticity, and large, reversible shape changes, which are promising for applications such as in artificial muscles,[19,37–40] soft robotics,[41,42] and reconfigurable structures.[14,17,18,43,44] The macroscopic shape change of LCEs relies on a reversible nematic–isotropic state transition of mesogens upon exposure to external stimuli (such as heat and light), which is tightly coupled with the alignment of mesogens.[45–47] Take LCEs synthesized by the two-stage thiol-acrylate Michael addition-photopolymerization (TAMAP) reaction for example, to program LCEs for actuation. LCEs are first aligned from a polydomain network into a monodomain (i.e., nematic

mesophase),[28,48] which is then permanently fixed via a second-stage photopolymerization, where additional crosslinking is induced. Typical alignment techniques include mechanical alignment,[17,49–54] surface alignment,[35,55] the use of external fields (electrical and magnetic),[56,57] and the recently developed direct ink writing (DIW) 3D printing.[31,58–62]

Existing efforts in creating LCE structures with various geometries and actuation behaviors have laid a solid foundation for the potential applications of LCEs. To further enhance their performance and to better mimic functionally gradient materials that are ubiquitous in biology and in engineering applications, LCEs with locally controlled properties are desired. Recently, a facile strategy was reported to print 3D LCE structures with graded properties by varying printing parameters.[63] It has also been revealed that the mesogen alignment, which is tightly coupled with the shape-morphing behavior of LCEs, is affected by the programmed strain.[64] Despite intensive studies, it remains largely unexplored how localized mesogen alignment and crosslinking densities at the molecular scale correlate with the mechanical properties at the material level and the shape-morphing behaviors at the structure level. Tailoring the morphing behaviors of LCEs via the local control of the molecular- and material-level properties would open up many opportunities for the applications of LCEs, such as variable stiffness for amphibious robots to operate in both aquatic and land environments.

Here we present a facile technique to create heterogeneous stiffness in morphing LCE structures via locally controlled photopolymerization and mechanical training. The approach exploits mechanical training,[65–70] including compressive buckling and folding, to achieve spatially aligned mesogens in the nematic state of LCEs based on the two-stage TAMAP reaction.[28,48] Applying a photomask during photopolymerization yields localized programming of LCE monodomains and highly crosslinked networks in the exposed regions. The Young's modulus of the light-exposed regions is found to be almost 50 times as large as that of the non-exposed ones, creating heterogeneous stiffness in a single 3D LCE structure. Heating and cooling across the isotropic clearing temperature (T_i) of LCEs induces the nematic–isotropic transition at the locally programmed regions, driving the shape morphing of the entire LCE structure. Highly integrated experimental and computational studies of systematically tailoring the shapes of a representative LCE ribbon structure illustrate the reliability of the proposed strategy. Furthermore, five 2D ribbons are mechanically trained into "UCONN" letter-like shapes via local photopolymerization, which can morph between their ribbon and letter shapes reversibly. The non-photopolymerized regions of LCE structures can be further sequentially programmed via local mechanical training and photopolymerization at the molecular level, resulting in multiple target shapes that can be actuated sequentially. The strategy can be further extended to a 3D LCE "face" formed through local molding and photopolymerization, which exhibits the sequential appearance of facial features. To summarize, the reported strategy based on mechanical training and locally controlled photopolymerization can enable the following salient features: (1) Formation of asymmetric, open-mesh 3D LCE structures with heterogeneous stiffness that are inaccessible with previous techniques; (2) sequential programming for repurposing or reshaping of structures by programming the lightly crosslinked regions; (3) creation of complaint, stretchable structures, as well as large, reversible shape morphing due to the softer lightly crosslinked region; and (4) ease of use, as well as being versatile, scalable, and compatible with existing mesogen alignment techniques. Harnessing the correlations between mesogen alignment and crosslinking at the molecular level and material properties and morphing behaviors at the material/structure level creates many opportunities for locally programmed LCE

[1]Department of Materials Science and Engineering, University of Connecticut, Storrs, CT 06259, USA

[2]Department of Chemistry, University of Connecticut, Storrs, CT 06269, USA

[3]Polymer Program, Institute of Materials Science, University of Connecticut, Storrs, CT 06259, USA

[4]Department of Mechanical and Aerospace Engineering, BioInspired Syracuse, Syracuse University, Syracuse, NY 13244, USA

[5]BioInspired Syracuse, Syracuse University, Syracuse, NY 13244, USA

[6]Lead contact

*Correspondence: tzhang48@syr.edu (T.Z.), xueju.wang@uconn.edu (X.W.)

https://doi.org/10.1016/j.matt.2022.08.019

Please cite this article in press as: Li et al., Morphing of stiffness-heterogeneous liquid crystal elastomers via mechanical training and locally controlled photopolymerization, Matter (2022), https://doi.org/10.1016/j.matt.2022.08.019

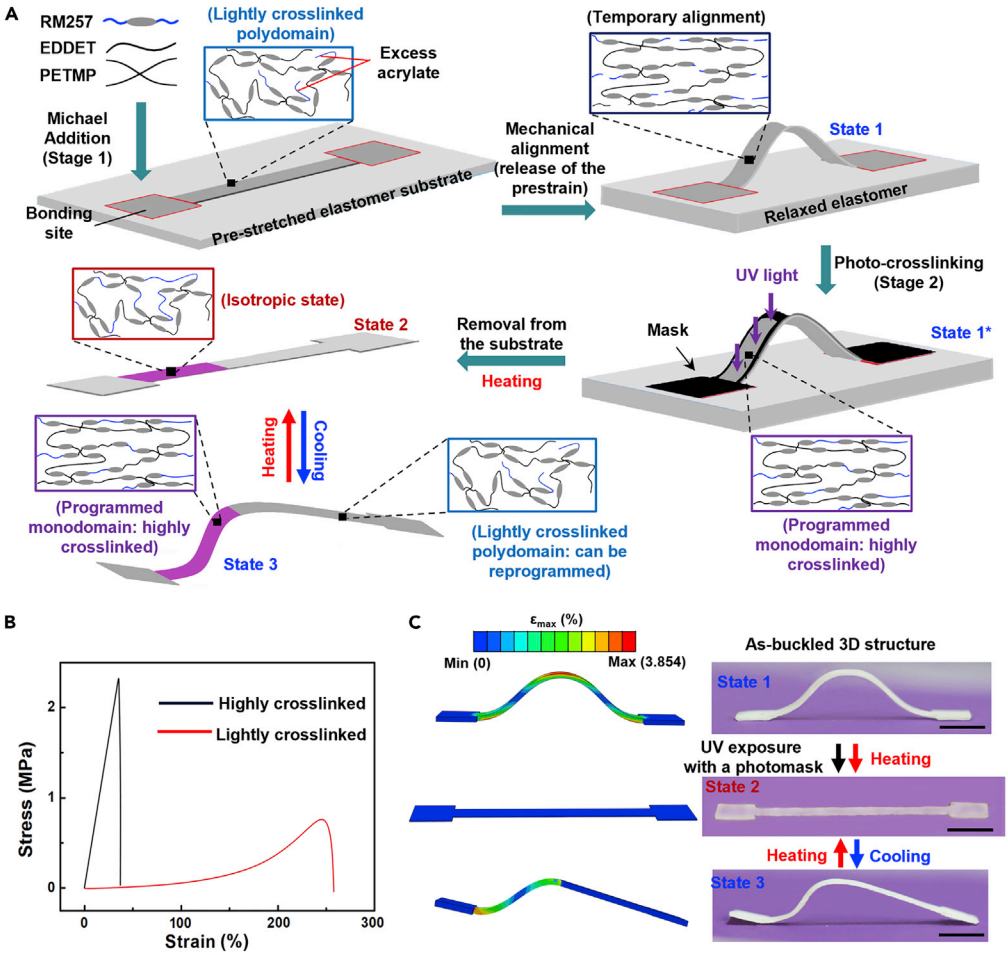

Figure 1. Stiffness-heterogeneous morphing LCE structures via local photopolymerization and mechanical training

(A) Schematic illustration of the fabrication and shape-morphing schemes of 3D LCE structures with heterogeneous stiffness, as well as the associated microscale mechanism.

(B) Stress-strain curves of lightly and highly crosslinked LCEs.

(C) FEA simulation and experimental results of the shape-morphing behavior of a 3D LCE ribbon structure after local photopolymerization and mechanical training. Scale bars, 2 mm. The strain refers to the maximum principal strain.

structures for potential applications in soft robotics, biomedical devices, and many others.

RESULTS

Tailoring the local crosslinking densities and stiffness of 3D LCE structures

Figure 1A schematically illustrates the fabrication and shape-morphing schemes of 3D LCE structures with heterogeneous stiffness. The procedure starts with the synthesis of LCE films using the TAMAP methodology.[28,48] Three major components are used in forming LCEs: (1) a structural component mesogen, 1,4-Bis-[4-(3-acryloyloxypropyloxy) benzoyloxy]-2-methylbenzene (RM257), which gives rise to the ordered LC phases; (2) a di-thiol monomoer 2,2-(ethylenedioxy) diethanethiol (EDDET); (3) a crosslinking monomer pentaerythritol tetrakis (3-mercaptopropionate) (PETMP). Mixing RM257, EDDET, and PETMP induces stage 1 reaction to form an initial, lightly crosslinked LCE polydomain network. Please note that a photoinitiator (2-hydroxyethoxy)-2-methylpropiophenone (HHMP) is also added to the solution to enable the

subsequent photopolymerization process. The lightly crosslinked polydomain LCE films are patterned into designed 2D geometries by using a CO_2 laser (VLS 2.30; Universal Laser System, Ansonia, CT) and then transferred onto a pre-stretched silicone elastomer substrate (Dragon Skin; Smooth-On, Easton, PA) as an assembly platform. An ultra-thin layer of superglue is applied to the 2D pattern at selective locations (bonding sites) to provide strong adhesion between the pattern and the substrate, while relatively weak van der Waals forces dominate the interface at all other locations. Release of the pre-strain in the elastomer substrate causes large compressive forces at the bonding sites, inducing in- and out-of-plane translations, and therefore geometrically transforms the 2D LCE pattern into a 3D structure (state 1). At the molecular level, the compressive strains induced during the buckling process spatially align mesogens into monodomains of ordered LC phases.

To create LCEs with heterogeneous stiffness, a photomask is used to selectively cover regions of LCE structures during the stage 2 photopolymerization, resulting in programmed, highly crosslinked monodomain regions (photopolymerized) and lightly crosslinked polydomain regions (non-photopolymerized) coexisting within one structure. For example, half of the ribbon structure is covered with a photomask (gray region, lightly crosslinked, denoted by LCE_{LXL}) while the other region is exposed (purple region, highly crosslinked, denoted by LCE_{HXL}). Ultraviolet light (UV) (wavelength: 365–400 nm) exposure initiates the stage 2 polymerization process in the purple region by inducing additional crosslinking, and permanently programs the aligned mesogen monodomains of the LCE, thereby "locking" the shape in this region. While in the gray region of the structure (LCE_{LXL}), which is covered by the photomask, lightly crosslinked LCEs are maintained. The difference in the crosslinking density and mesogen alignment in the two regions results in heterogeneous stiffness within one structure (state 1*). To quantify their stiffness, highly crosslinked and lightly crosslinked LCE samples are patterned into a dimension of 25 × 15 × 1 mm using a CO_2 laser and tested using a tensile tester (MTEST Quattro; ADMET Inc., Norwood, MA) at a displacement rate of 0.01 mm s^{-1}. The Young's modulus of the highly crosslinked LCE is measured to be 6.09 MPa, which is about 48 times as large as that of the lightly crosslinked LCE (0.126 MPa), as shown in Figure 1B. This distinct difference in modulus and mesogen alignment between the LCE_{HXL} and LCE_{LXL} regions creates locally heterogeneous stiffness and governs the morphing of LCE structures, which is discussed below.

After the structure is removed from the substrate, heating above the isotropic clearing temperature (T_i = 62°C in this study) disrupts the LC molecular order in the nematic state (purple region) and drives the 3D LCE structure to return to its 2D configuration (state 2).[28] When it cools down, isotropic-nematic state transition occurs in the LCE_{HXL} (purple) region, driving the whole structure to morph into its 3D shape. The stiffness and mesogen alignment heterogeneity can yield an interesting asymmetric structure, which is difficult to achieve via existing alignment techniques, including surface patterning[35,55] and 3D printing.[31,58–61] The nematic-to-isotropic transition at the LCE_{HXL} region can be reversibly achieved via heating and cooling across T_i, thereby enabling the macroscopic reversible shape-switching capability of the asymmetric 3D LCE structure. Please note that the lightly crosslinked polydomain region can be further programmed for multipurpose functionality, which is discussed in the section "Diverse stiffness-heterogeneous morphing LCE structures".

Figures 1C and S1 present experimental and quantitative finite element analysis (FEA) of the configurations of a representative LCE ribbon structure corresponding to different states in the schematic illustration of Figure 1A. The color bar denotes

maximum principal strain distributions within the structure. The as-buckled LCE ribbon structure adopts an arc shape. After selective photopolymerization using a photomask, it is partially programmed and can return to its 2D configuration upon heating above 62°C. This 2D ribbon can morph into an asymmetric 3D shape resulting from locally controlled heterogeneous stiffness and spatial mesogen alignment when it cools below 62°C, as shown in Video S1. The shape changes between the 2D pattern and the asymmetric 3D shape are reversible due to the reversible nematic-isotropic state transition of mesogens in the programmed LCE_{HXL} regions. In addition, we perform polarized light microscopy imaging (Olympus BX51P microscope) to determine the presence of liquid crystalline textures in pristine, uniaxially stretched, and buckled LCE samples. Please note that the pristine and uniaxially stretched samples are imaged here as a reference. Figure S2 shows that the pristine LCE samples without any processing do not reveal liquid crystalline textures at 25°C, while the uniaxially stretched LCE samples reveal the presence of liquid crystalline birefringent textures at 25°C with some degree of alignment. Similar observations are made for buckled LCE structures (corresponding to state 3 in Figure 1C) imaged at 25°C (Figure S3). Birefringence from the local ordering of liquid crystalline domains at various sites indicates the influence of compressive forces on the local alignment of mesophases.

Modeling of the shape-morphing behavior in the stiffness-heterogeneous LCE structure is conducted based on a Saint-Venant-Kirchhoff model. The shape fixing and stiffening in the programmed, highly crosslinked region (highlighted in purple) are achieved by a "model change" feature in Abaqus.[71] More specifically, the 2D pattern is designed with two regions and have a uniform ground state modulus of 0.126 MPa, corresponding to the lightly crosslinked polydomain state of LCEs after stage 1 reaction. The entire structure is then compressively buckled into a 3D shape simulated by using 3D elements. The meshes are then removed and reactivated, and set to be stress-free through the "model change" feature. The modulus of the highly crosslinked region is then set to be 6.09 MPa based on the experimental measurement results in Figure 1B, to capture the modulus change from lightly to highly crosslinked regions after stage 2 photopolymerization. Please note that the effect of buckling-induced heterogeneous strain distributions on the stiffness is not considered here. Despite this simplification, the modeling results are shown to be highly consistent with the experimental observations, which demonstrate that the experimentally informed model is very promising in predicting the shape-morphing behavior under stiffness heterogeneity. In addition, we studied the effect of modulus ratios between the highly crosslinked (LCE_{HXL}) and lightly crosslinked (LCE_{LXL}) regions by setting $E_{LCE_{HXL}}/E_{LCE_{LXL}} = 5, 35, 100$ respectively. Figure S4 shows the FEA predictions for the final configurations (nematic state) under these modulus ratios. The color bar represents the maximum principal strain distribution. The results show that as the modulus ratio increases, the structure has a better capability for shape fixing, due to the stiffer portion of the structure. Eventually, the structure reaches to a converged configuration and does not show significant changes with a further increase of the modulus ratio.

We further study the effect of localized mesogen alignment and crosslinking densities as well as the resulting heterogeneous stiffness on the configuration and morphing behavior of the ribbon structure by varying the location and the areas of lightly and highly crosslinked LCE regions. Figure 2 presents a collection of experimental results and FEA predictions for various mechanically trained 3D LCE ribbon structures, where selective UV exposure of the buckled structure yields both symmetric and asymmetric 3D shapes of varying degrees of deformation. As shown in

Please cite this article in press as: Li et al., Morphing of stiffness-heterogeneous liquid crystal elastomers via mechanical training and locally controlled photopolymerization, Matter (2022), https://doi.org/10.1016/j.matt.2022.08.019

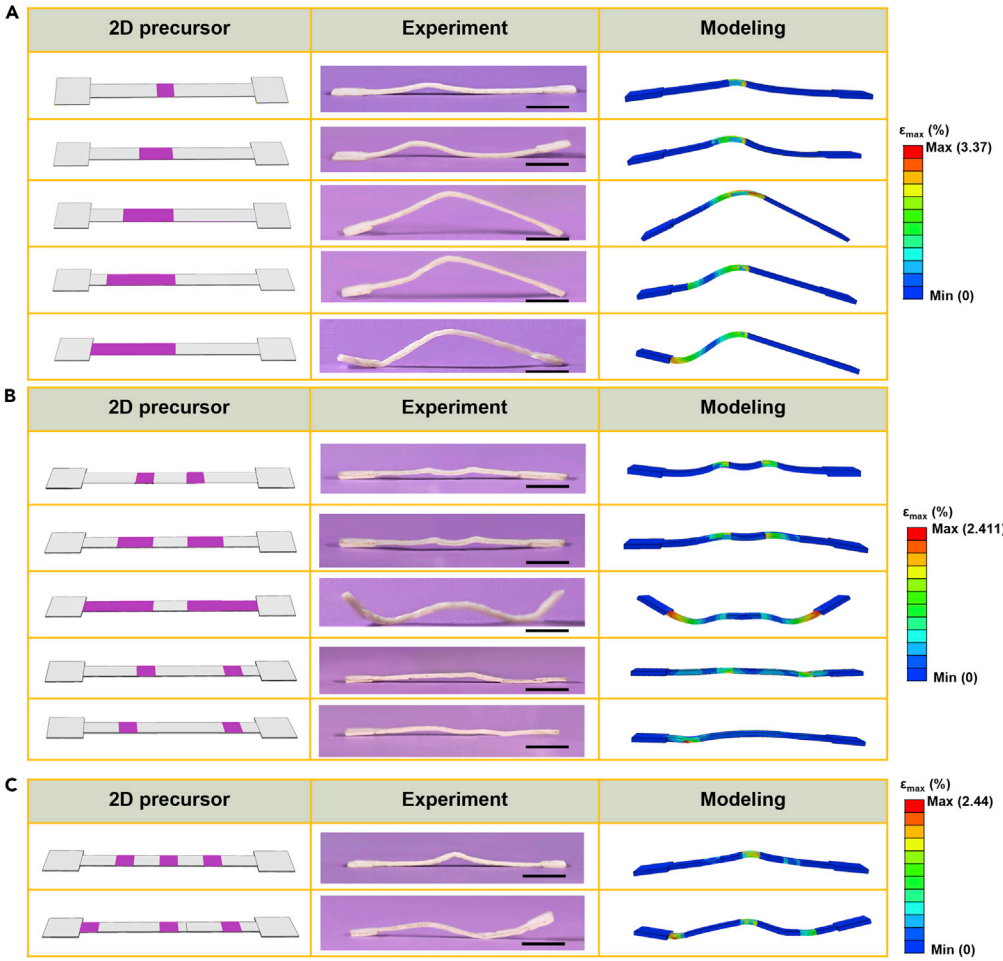

Figure 2. A collection of experimental results and FEA predictions for locally programmed and mechanically trained 3D LCE ribbon structures, where heterogeneous stiffness of the buckled structure yields both symmetric and asymmetric 3D shapes of varying degrees of deformation

(A) LCEs with one locally programmed region of increasing areas.

(B) LCEs with two symmetric locally programmed regions.

(C) LCEs with three locally programmed regions. Scale bars in (A)–(C), 2 mm. The purple regions are UV exposed and highly crosslinked. The strain refers to the maximum principal strain.

Figure 2A, enlarging the UV exposed area in the left half of the 3D LCE ribbon structure increases the area of the highly crosslinked (larger stiffness) and the "locked" mesogen alignment region, and therefore enhances the deformation degree of the whole structure, leading to various asymmetric 3D shapes. Furthermore, extending the UV exposed area to two separate sections in a symmetric manner, as shown in the first three structures in Figure 2B, yields various symmetric 3D shapes with different degrees of deformation. Due to the design flexibility of the photomask, rearranging these two UV exposed regions to break their symmetry (last two structures in Figure 2B) results in asymmetric geometries. These results show that the configuration and the degree of symmetry/asymmetry of the ribbon structure can be tailored by tuning the location and area of the UV exposed region and therefore the crosslinking density and mesogen alignment in the structure. In addition, Figure 2C shows that increasing the number of UV exposed segments can further increase the complexity of the resulting structure. These results demonstrate that tailoring the local crosslinking density and mesogen alignment at the molecular level

Please cite this article in press as: Li et al., Morphing of stiffness-heterogeneous liquid crystal elastomers via mechanical training and locally controlled photopolymerization, Matter (2022), https://doi.org/10.1016/j.matt.2022.08.019

of LCEs via a series of mechanical trainings and selective photopolymerizations can tune the stiffness of LCEs at the material level, which then synergistically control the shape-morphing behavior of 3D LCE structures. Such molecular-material-structure interactions can be harnessed to design various symmetric/asymmetric geometries of LCE structures with heterogeneous stiffness distributions, which are difficult to achieve via previous approaches, such as direct 3D buckling[17] and direct ink writing (DIW) 3D printing.[31,59–61]

Diverse stiffness-heterogeneous morphing LCE structures

Our approach can also be extended to create more complex structures with locally varying stiffness (Figures 3A–3C and Figure S5). As shown in Figure 3A, local UV exposure of one crossed beam (purple region) in a buckled structure consisting of four ribbons "locks" the local mesogen alignment and creates higher stiffness in the crossed beam region, which drives the morphing of the whole structure into an asymmetric 3D configuration under thermal actuation. Selective UV exposure of two symmetric crossed beams (purple regions) results in a symmetric 3D configuration. Furthermore, Figure 3B shows that selective UV exposure of the inner and outer layers of a flower-like structure presents different flower-blooming states. This concept can be applied not only to the design of plant-inspired structures, but also to that of animal-inspired structures, as shown in Figure 3C. UV exposure of different regions of an insect-like structure (the entire structure, half of the structure, and the entire structure except two "legs," respectively) leads to three configurations that resemble various standing states of an "insect," respectively. These results demonstrate the potential applications of this strategy in assembling biomimetic structures and devices.

In addition to being programmed by mechanical buckling, the developed approach also applies to LCEs trained by other mechanical deformation modes, such as bending. Figure 3D shows local programming (purple regions) of five LCE ribbon structures into various "letter" shapes, demonstrating "UCONN" (abbreviation for the University of Connecticut). The structures can achieve reversible shape morphing between the straight ribbon and "UCONN" configurations upon heating and cooling across 62°C.

Sequential programming of LCE ribbon structures

The lightly crosslinked, "unlocked" polydomain region in locally programmed LCE structures can be further programmed for multipurpose functionality, which opens routes to additional classes of LCE structures. As shown in Figure 4, we use a ribbon structure as an example to demonstrate this approach. A square mold fabricated from a soft elastomer, polydimethylsiloxane (PDMS) (1 mm thick), is used to perform the mechanical training and sequential programming of LCE structures by folding the LCE ribbon to the shape of the mold (Figure 4A). In the first step of programming, we perform local UV exposure to the top left (first) corner of the LCE square by using a photomask. After being removed from the mold and being heated above T_i = 62°C, the LCE structure recovers its straight ribbon configuration due to the nematic-to-isotropic state transition at the programmed left corner region. Cooling down to room temperature morphs it into a right-angle configuration fixed by the programmed corner (Figure 4B). The transition between the straight ribbon and right-angle configuration can be reversibly achieved via heating and cooling across 62°C. In order to conduct the second step of programing to lock the other local part of this LCE structure, we remold the LCE ribbon in the right-angle configuration to a square shape, and then perform local UV light exposure for the top right (second) corner of the LCE square. The structure recovers the straight ribbon shape when

Please cite this article in press as: Li et al., Morphing of stiffness-heterogeneous liquid crystal elastomers via mechanical training and locally controlled photopolymerization, Matter (2022), https://doi.org/10.1016/j.matt.2022.08.019

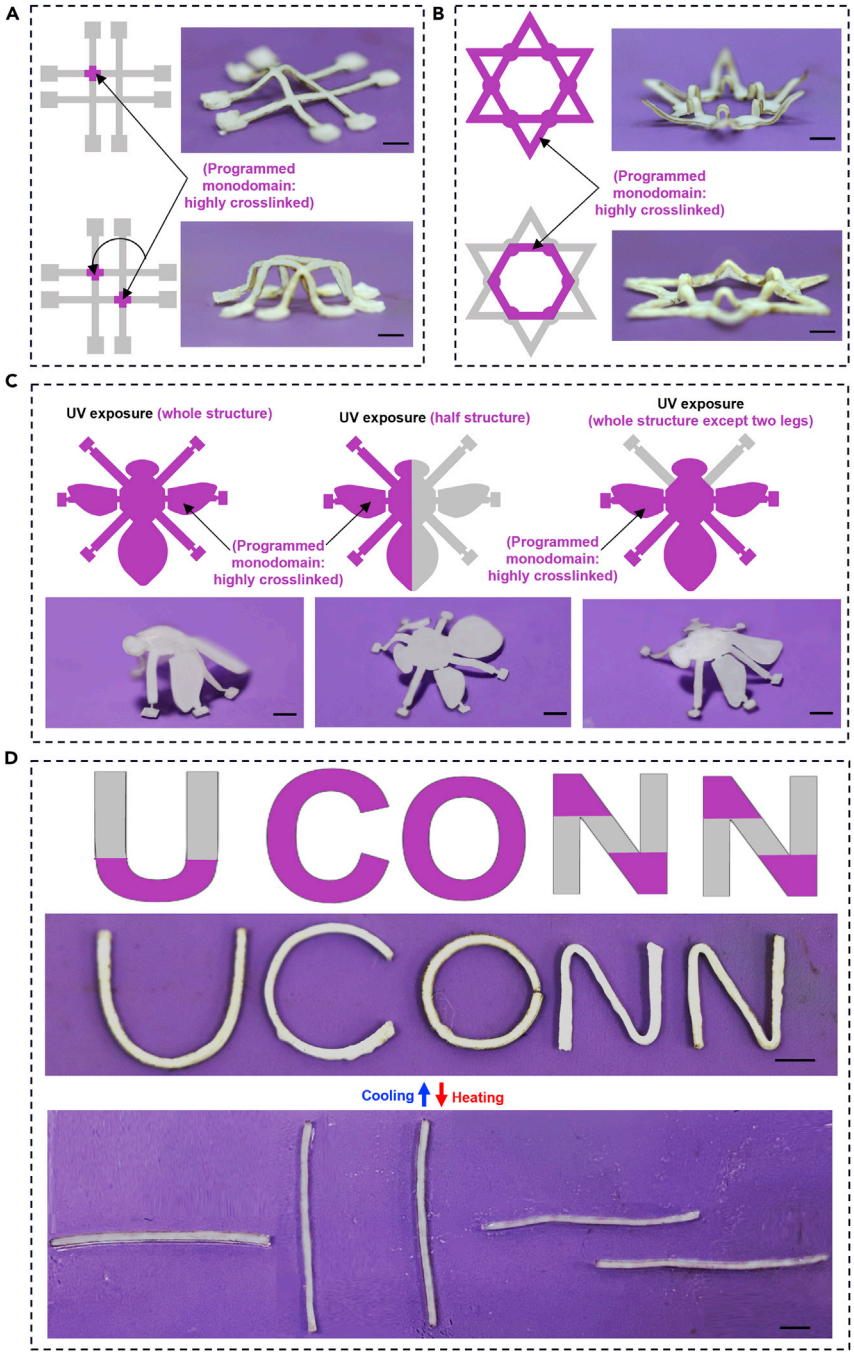

Figure 3. Experimental results of mechanically trained complex LCE structures with heterogeneous stiffness

(A) Crossed beam structures with different UV exposed regions.

(B) Flower-like structures that present different flower-blooming states via selective UV exposure of their inner and outer layers.

(C) Various programmed configurations of an insect-like structure via selective UV exposure of different regions.

(D) Locally programmed five LCE ribbon structures that resemble various "letter" shapes, demonstrating "UCONN" (abbreviation for the University of Connecticut). Scale bars in (A)–(D), 3 mm. The purple region in each structure corresponds to the highly crosslinked region in LCEs.

Please cite this article in press as: Li et al., Morphing of stiffness-heterogeneous liquid crystal elastomers via mechanical training and locally controlled photopolymerization, Matter (2022), https://doi.org/10.1016/j.matt.2022.08.019

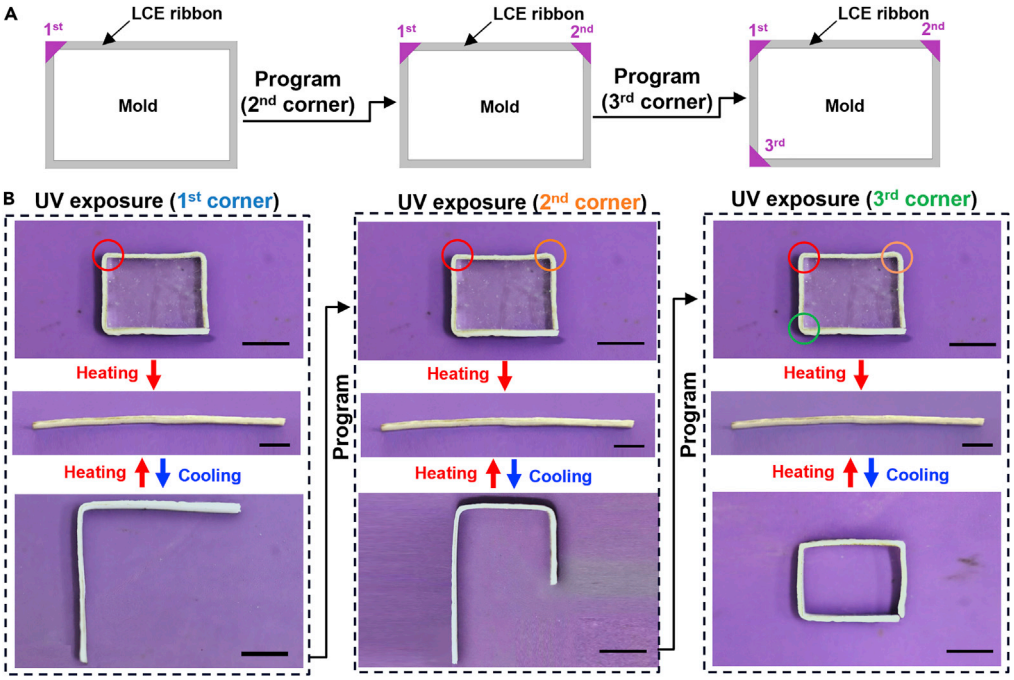

Figure 4. Sequential programming of LCE structures

(A) Schematic illustration of the sequential programming process using a square mold.

(B) Optical images of the programmed ribbon by folding it around the square mold and UV exposure of the first, second, and third corners, respectively. After each programing step, the 3D-2D reconfiguration of the ribbon structure can be achieved reversibly under thermal actuation. Scale bars, 2 mm.

being heated above 62°C. Cooling down to room temperature yields a double-right-angle configuration fixed by the two programmed corners, showing the effect of programming the second corner. The third step of programing the LCE structure is implemented on the left lower (third) corner of this structure, resulting in a square configuration after heating and cooling across 62°C. This sequential programming approach enables multiple reconfigurations of the same structure, which can be harnessed for multipurpose applications.

Reshaping of a 3D LCE "face"

The reversible shape-shifting and sequential programing capabilities of LCEs make it promising for many applications, including in artificial skins and muscles. Figure 5 displays the process of creating an LCE structure in a "face" shape that can sequentially exhibit different facial features. In Figure 5A, a lightly crosslinked LCE membrane (150 μm thick) resulting from stage 1 reaction is laminated onto a face mold (plastic toy doll, Amazon) to mechanically align mesogens into monodomains. The aligned LCE is then exposed to UV light for 6 min to induce stage 2 reaction and enable the permanent programming of the ordered monodomain. Such processing procedure leads to an LCE membrane with programmed facial features. When heated above T_i = 62°C, the LCE returns to a planar configuration, where facial features disappear, due to the nematic-to-isotropic state transition. Upon cooling down, the facial features appear because of the reversible state transition to the nematic state of LCEs. In addition, by adopting the sequential programming technique introduced in Sequential programming of LCE ribbon structures, we can selectively display the facial features, as shown in Figure 5B and Videos S2, S3, and S4. After the LCE membrane is conformally laminated onto the "face" mold, through a photomask, the nose portion is first UV exposed

Please cite this article in press as: Li et al., Morphing of stiffness-heterogeneous liquid crystal elastomers via mechanical training and locally controlled photopolymerization, Matter (2022), https://doi.org/10.1016/j.matt.2022.08.019

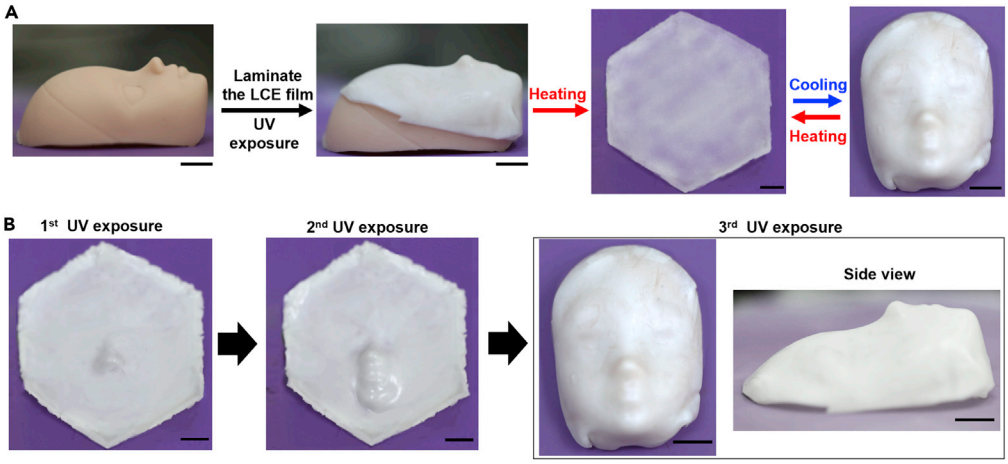

Figure 5. Sequential programming of an LCE membrane into a "face" shape that exhibits different facial features

(A) Programming and shape morphing of an LCE membrane into a "face" shape via molding and photopolymerization.

(B) An LCE membrane in a "face" shape that can exhibit different facial features by sequentially programming "nose," "mouth," and "eyes" via local photopolymerization and molding. After each programing step, the 3D-2D reconfiguration of the membrane can be achieved reversibly under thermal actuation. Scale bars in (A)–(B), 5 mm.

and permanently programmed, followed by the mouth, and then the eyes. After each programming step, the formed LCE structure can be heated above T_i = 62°C to enable the nematic–isotropic state transition of the LCEs and reconfigure the corresponding 3D shape into its original 2D configuration. These results showcase the potential for using molds to sequentially program the facial expressions of a "face" model for selective and sequential display.

DISCUSSION

In summary, the results presented here demonstrate a facile and effective technique for realizing stiffness-heterogeneous and locally controlled reconfigurable LCE structures via mechanical training and local photopolymerization. More specifically, tailoring the local crosslinking density and mesogen alignment at the molecular level of LCEs tunes the stiffness at the material level, which then synergistically controls the shape-morphing behavior at the structure level. Experiments integrated with quantitative FEA results systematically present a rich range of symmetric/asymmetric geometries by harnessing the molecular-material-structure interactions in a mechanically trained LCE structure, which illustrates the basic ideas and validates the strategy. Additional demonstrations of complex 3D LCE structures, including those that resemble flowers and insects with heterogeneous stiffness distributions as well as their large, reversible shape-morphing behaviors, show reliability of our strategy. Furthermore, programming LC molecules in the lightly crosslinked regions of LCE structures provides a promising strategy to enrich the design space and potential applications of reconfigurable LCE structures for multipurpose functionalities. The demonstrated sequentially programmed LCE "face" that can achieve multiple facial features in a well-controlled, sequential manner via spatially programing LC molecules highlights potential applications in artificial faces and many others. Future directions include incorporating adaptable network polymers[72] to allow for the reprogrammability of the material. In addition, by integrating multi-functional materials and electronics into locally programmed LCEs, it is possible to achieve distributed actuation and sensing for shape-changing robots with heterogeneous stiffness to accommodate operation in both land and underwater environments.

Please cite this article in press as: Li et al., Morphing of stiffness-heterogeneous liquid crystal elastomers via mechanical training and locally controlled photopolymerization, Matter (2022), https://doi.org/10.1016/j.matt.2022.08.019

EXPERIMENTAL PROCEDURES

Resource availability

Lead contact

Further information and requests for resources and materials should be directed to and will be fulfilled by the lead contact, Xueju Wang (xueju.wang@uconn.edu).

Materials availability

This study did not generate new unique reagents.

Data and code availability

The experimental and modeling data that support the findings of this study have been deposited at https://doi.org/10.5281/zenodo.6908624.

Synthesis of LCE films

A two-stage TAMAP methodology[28,48] was used for the synthesis of LCEs in this study. 1,4-Bis-[4-(3-acryloyloxypropyloxy) benzoyloxy]-2-methylbenzene (RM257) was acquired from Wilshire Technologies Inc. and used as procured, without any extra purification. EDDET (a di-thiol monomer), PETMP (a tetra-functional thiol cross-linking monomer), (2-hydroxyethoxy)-2-methylpropiophenone (HHMP), dipropylamine (DPA), and toluene were acquired from Sigma-Aldrich and were also used as received. To start the synthesis, 40 wt% of toluene was added to RM257 (powder) and heated at a temperature of 80°C to dissolve RM257. After cooling to room temperature, EDDET and PETMP with a molar ratio of 15:85 (EDDET:PETMP) were added to the solution to initiate the step 1 reaction. Furthermore, 0.38 wt% of HHMP, a photoinitiator, was added to the solution to facilitate the subsequent photopolymerization reaction. Meanwhile, a solution of diluted DPA in toluene with a molar ratio of 1:50 was separately prepared to act as a catalyst when added to the monomer solution. Next, the solution was mixed using a planetary mixer (AR-100, Thinky) at 2000 rpm for 30 s, and air bubbles were then deformed for another 30 s. The solution was then spin coated onto a high-density polyethylene substrate at 200 to 1,000 rpm for 20 s to create LCE films of differing thicknesses. Finally, the films were cured at room temperature for 12 h, and then placed in a vacuum chamber at 80°C for 12 h to completely evaporate the toluene.

Compressive buckling

With a CO_2 laser (VLS 2.3; University Laser System, Ansonia, CT), desired geometries were patterned out of the synthesized LCE films and were then laminated onto a pre-stretched silicone elastomer substrate (Dragon Skin; Smooth-On, Easton, PA) as an assembly platform. A thin layer of superglue was applied to the bond sites of the 2D patterns to form strong adhesion between the pattern and the substrate only at these locations. Releasing the pre-strain in the elastomer substrate induced compressive buckling and geometrical transformation of the 2D patterns into 3D structures. During this process, mesogens were spatially aligned into their monodomains due to the compressive strain.

Local programming and reversible shape changes of 3D LCE structures

To locally "lock" the ordered LCE monodomains, the buckled 3D LCE structure was covered with a photomask that was fabricated from an opaque black glove using a CO_2 laser, and exposed to UV light (wavelength: 365 to 400 nm) for 6 min for photopolymerization. The locally programmed 3D structure was then removed from the elastomer substrate and heated above T_i = 62°C, which caused the nematic–isotropic transition of the permanently programmed LC phases in the "locked" regions of the 3D LCE structure and therefore reconfigured the structure into its

Please cite this article in press as: Li et al., Morphing of stiffness-heterogeneous liquid crystal elastomers via mechanical training and locally controlled photopolymerization, Matter (2022), https://doi.org/10.1016/j.matt.2022.08.019

original 2D pattern. Once the LCE cooled to room temperature, the 2D configuration morphed to a 3D shape that was determined by the local programming.

Finite element analysis

Finite element modeling was performed by using the commercial software ABAQUS/Implicit. The standard 3D stress element type with linear geometric order (C3D8R) was used for simulating the compressive buckling of LCE patterns. We refined meshes to ensure computational accuracy and identified the optimum mesh size to balance the computational cost and simulation accuracy. Mesh distortion control and enhanced hourglass control were used to help the convergence of the nonlinear simulations. The following elastic moduli (E) and Poisson's ratio (ν) values were used for the simulation of LCEs in their different states (original state and nematic state): $E_{LCE\ (original)}$ = 0.126 MPa, $\nu_{LCE\ (original)}$ = 0.45; $E_{LCE(nematic)}$ = 6.09 MPa, $\nu_{LCE\ (nematic)}$ = 0.45, with the moduli determined from the stress-strain curves measured in experiments. To simplify the model, we assumed the LCE followed the Saint Venant-Kirchhoff material constitutive law. We modeled the shape changes of locally programmed LCE structures via three steps. In the first step, a uniform LCE film with $E_{LCE\ (original)}$ and $\nu_{LCE\ (original)}$ was compressively buckled into a 3D configuration. In the second step, "model change" interactions were applied to the UV exposed regions of LCEs. The "model change" re-defined the stress-free configurations as the buckled state and changed the modulus from 0.126 MPa to 6.09 MPa in the UV exposed region, thereby achieving local shape fixing and material stiffening. Finally, the boundary conditions for buckling were released. The non-UV-exposed LCE (original state) portion tends to return to the 2D configuration, while the locally programmed LCE (nematic state) portion prefers to keep the buckled shape. Their competition drives the morphing of the entire structure into a 3D shape. Although the constitutive model used here is simpler than that for the LCE, which usually exhibits anisotropic properties associated with the mesogen alignment,[73,74] it captures the key factors for the shape morphing, including the local shape locking and modulus increase. In addition, the ribbon structures and their assembly usually have a well-defined bending direction, making their shape changes insensitive to material anisotropies. We expect the anisotropic material properties of LCEs will play more important roles in the 2D sheet morphing, such as the "face" shown in Figure 5 and will explore this in our future studies.

Programming LCEs via molds

The molds used for creating structures in Figures 3D and 4 were fabricated by patterning PDMS (1 mm thick) into desired geometries with a CO_2 laser (VLS 2.30; University Laser System, Ansonia, CT). To program LCEs with the molds, LCE ribbons were cut and laminated onto the mold, where the adhesion between the LCE ribbon and the PDMS mold was governed by van der Waals forces.

To fabricate LCE "UCONN" letters, PDMS molds that resembled those five letters were first created. Five individual ribbons were deformed to the "UCONN" letter shapes, respectively, with the assistance of the molds. Selective UV exposure with a photomask induced photopolymerization. Detaching the ribbons from the mold formed the shapes of "UCONN." Heating and cooling across 62°C caused the morphing between straight ribbons and "UCONN" letters.

To program the ribbon structure in Figure 4A, a square PDMS mold was created. The ribbon was laminated around the mold, and a photomask was applied to the ribbon with only the left-up corner exposed. UV exposure permanently programmed the ordered monodomain in the exposed region. The LCE ribbon was then detached from

the mold. Heating and cooling across 62°C resulted in a right-angle configuration due to local fixing. The same procedure was repeated to program other corners of the ribbon and the associated shapes.

SUPPLEMENTAL INFORMATION

Supplemental information can be found online at https://doi.org/10.1016/j.matt.2022.08.019.

ACKNOWLEDGMENTS

Y.L. and X.J.W. acknowledge the support from the National Science Foundation (NSF) (Grant No. CAREER CMMI 2144687 and CMMI 2103012). T.Z. thanks the NSF (Grant No. CMMI 2020476) for their support.

AUTHOR CONTRIBUTIONS

X.W. conceived the idea and supervised the experiments. Y.L. and G.P. conducted the experiments on the fabrication and testing of liquid crystal elastomer structures with local programming and polymerization. F.M. and R.K. performed the study of mesogen alignment. T.Z. and Y.L. conducted the finite element modeling. X.W., Y.L., and T.Z. wrote the manuscript. All authors discussed and commented on the manuscript.

DECLARATION OF INTERESTS

The authors declare no competing interests.

Received: May 4, 2022
Revised: June 29, 2022
Accepted: August 16, 2022
Published: September 5, 2022

REFERENCES

1. Gladman, A.S., Matsumoto, E.A., Nuzzo, R.G., Mahadevan, L., and Lewis, J.A. (2016). Biomimetic 4D printing. Nat. Mater. *15*, 413–418. https://doi.org/10.1038/Nmat4544.

2. Breger, J.C., Yoon, C., Xiao, R., Kwag, H.R., Wang, M.O., Fisher, J.P., Nguyen, T.D., and Gracias, D.H. (2015). Self-folding thermo-magnetically responsive soft microgrippers. ACS Appl. Mater. Interfaces *7*, 3398–3405. https://doi.org/10.1021/am508621s.

3. Zhao, Q., Zou, W., Luo, Y., and Xie, T. (2016). Shape memory polymer network with thermally distinct elasticity and plasticity. Sci. Adv. *2*, e1501297. https://doi.org/10.1126/sciadv.1501297.

4. Lendlein, A., and Gould, O.E.C. (2019). Reprogrammable recovery and actuation behaviour of shape-memory polymers. Nat. Rev. Mater. *4*, 116–133. https://doi.org/10.1038/s41578-018-0078-8.

5. Liu, Y., Shaw, B., Dickey, M.D., and Genzer, J. (2017). Sequential self-folding of polymer sheets. Sci. Adv. *3*, e1602417. https://doi.org/10.1126/sciadv.1602417.

6. Liu, Y., Boyles, J.K., Genzer, J., and Dickey, M.D. (2012). Self-folding of polymer sheets using local light absorption. Soft Matter *8*, 1764–1769. https://doi.org/10.1039/C1SM06564E.

7. Pelrine, R., Kornbluh, R., and Kofod, G. (2000). High-strain actuator materials based on dielectric elastomers. Adv. Mater. *12*, 1223–1225. https://doi.org/10.1002/1521-4095(200008)12:16<1223::AID-ADMA1223>3.0.CO;2-2.

8. Hajiesmaili, E., and Clarke, D.R. (2019). Reconfigurable shape-morphing dielectric elastomers using spatially varying electric fields. Nat. Commun. *10*, 183–187. https://doi.org/10.1038/s41467-018-08094-w.

9. Kim, Y., Yuk, H., Zhao, R., Chester, S.A., and Zhao, X. (2018). Printing ferromagnetic domains for untethered fast-transforming soft materials. Nature *558*, 274–279. https://doi.org/10.1038/s41586-018-0185-0.

10. Boncheva, M., Andreev, S.A., Mahadevan, L., Winkleman, A., Reichman, D.R., Prentiss, M.G., Whitesides, S., and Whitesides, G.M. (2005). Magnetic self-assembly of three-dimensional surfaces from planar sheets. Proc. Natl. Acad. Sci. USA *102*, 3924–3929. https://doi.org/10.1073/pnas.0500807102.

11. Kim, Y., Parada, G.A., Liu, S., and Zhao, X. (2019). Ferromagnetic soft continuum robots. Sci. Robot. *4*, eaax7329. https://doi.org/10.1126/scirobotics.aax7329.

12. Hu, W., Lum, G.Z., Mastrangeli, M., and Sitti, M. (2018). Small-scale soft-bodied robot with multimodal locomotion. Nature *554*, 81–85. https://doi.org/10.1038/nature25443.

13. Traugutt, N.A., Mistry, D., Luo, C., Yu, K., Ge, Q., and Yakacki, C.M. (2020). Liquid-crystal-elastomer-based dissipative structures by digital light processing 3D printing. Adv. Mater. *32*, e2000797. https://doi.org/10.1002/adma.202000797.

14. Wei, Z., and Bai, R. (2022). Temperature-modulated photomechanical actuation of photoactive liquid crystal elastomers. Extreme Mech. Lett. *51*, 101614. https://doi.org/10.1016/j.eml.2022.101614.

15. Kim, S.U., Lee, Y.J., Liu, J., Kim, D.S., Wang, H., and Yang, S. (2022). Broadband and pixelated camouflage in inflating chiral nematic liquid crystalline elastomers. Nat. Mater. *21*, 41–46. https://doi.org/10.1038/s41563-021-01140-x.

16. Guin, T., Settle, M.J., Kowalski, B.A., Auguste, A.D., Beblo, R.V., Reich, G.W., et al. (2018). Layered liquid crystal elastomer actuators. Nat. Commun. *9*, 2531. https://doi.org/10.1038/s41467-018-04911-4.

17. Li, Y., Yu, H., Yu, K., Guo, X., and Wang, X. (2021). Reconfigurable three-dimensional mesostructures of spatially programmed liquid crystal elastomers and their ferromagnetic composites. Adv. Funct. Mater. *31*, 2100338. https://doi.org/10.1002/adfm.202100338.

18. Li, Y., Luo, C., Yu, K., and Wang, X. (2021). Remotely controlled, reversible, on-demand assembly and reconfiguration of 3D mesostructures via liquid crystal elastomer platforms. ACS Appl. Mater. Interfaces *13*, 8929–8939. https://doi.org/10.1021/acsami.0c21371.

19. Ware, T.H., McConney, M.E., Wie, J.J., Tondiglia, V.P., and White, T.J. (2015). Voxelated liquid crystal elastomers. Science *347*, 982–984. https://doi.org/10.1126/science.1261019.

20. Cianchetti, M., Laschi, C., Menciassi, A., and Dario, P. (2018). Biomedical applications of soft robotics. Nat. Rev. Mater. *3*, 143–153. https://doi.org/10.1038/s41578-018-0022-y.

21. Li, R., Wang, L., and Yin, L. (2018). Materials and devices for biodegradable and soft biomedical electronics. Materials *11*. https://doi.org/10.3390/ma11112108.

22. Joo, H., Lee, Y., Kim, J., Yoo, J.-S., Yoo, S., Kim, S., Arya, A.K., Kim, S., Choi, S.H., Lu, N., et al. (2021). Soft implantable drug delivery device integrated wirelessly with wearable devices to treat fatal seizures. Sci. Adv. *7*, eabd4639. https://doi.org/10.1126/sciadv.abd4639.

23. Fortunato, G., Tatsi, E., Corsini, F., Turri, S., and Griffini, G. (2020). Stimuli-responsive luminescent solar concentrators based on photoreversible polymeric systems. ACS Appl. Polym. Mater. *2*, 3828–3839. https://doi.org/10.1021/acsapm.0c00515.

24. Zhu, R., Zhang, Z., and Li, Y. (2019). Advanced materials for flexible solar cell applications. Nanotechnol. Rev. *8*, 452–458. https://doi.org/10.1515/ntrev-2019-0040.

25. Zhang, Y., Wang, Z., Yang, Y., Chen, Q., Qian, X., Wu, Y., et al. (2020). Seamless multimaterial 3D liquid-crystalline elastomer actuators for next-generation entirely soft robots. Sci. Adv. *6*, eaay8606. https://doi.org/10.1126/sciadv.aay8606.

26. Shahsavan, H., Aghakhani, A., Zeng, H., Guo, Y., Davidson, Z.S., Priimagi, A., and Sitti, M. (2020). Bioinspired underwater locomotion of light-driven liquid crystal gels. Proc. Natl. Acad. Sci. USA *117*, 5125–5133. https://doi.org/10.1073/pnas.1917952117.

27. White, T.J., and Broer, D.J. (2015). Programmable and adaptive mechanics with liquid crystal polymer networks and elastomers. Nat. Mater. *14*, 1087–1098. https://doi.org/10.1038/nmat4433.

28. Saed, M.O., Torbati, A.H., Nair, D.P., and Yakacki, C.M. (2016). Synthesis of programmable main-chain liquid-crystalline elastomers using a two-stage thiol-acrylate reaction. JoVE, e53546. https://doi.org/10.3791/53546.

29. Saed, M.O., Volpe, R.H., Traugutt, N.A., Visvanathan, R., Clark, N.A., and Yakacki, C.M. (2017). High strain actuation liquid crystal elastomers via modulation of mesophase structure. Soft Matter *13*, 7537–7547. https://doi.org/10.1039/c7sm01380a.

30. Pei, Z., Yang, Y., Chen, Q., Terentjev, E.M., Wei, Y., and Ji, Y. (2014). Mouldable liquid-crystalline elastomer actuators with exchangeable covalent bonds. Nat. Mater. *13*, 36–41. https://doi.org/10.1038/nmat3812.

31. Kotikian, A., Truby, R.L., Boley, J.W., White, T.J., and Lewis, J.A. (2018). 3D printing of liquid crystal elastomeric actuators with spatially programed nematic order. Adv. Mater. 30. https://doi.org/10.1002/adma.201706164.

32. Maeng, J., Rihani, R.T., Javed, M., Rajput, J.S., Kim, H., Bouton, I.G., Criss, T.A., Pancrazio, J.J., Black, B.J., and Ware, T.H. (2020). Liquid crystal elastomers as substrates for 3D, robust, implantable electronics. J. Mater. Chem. B *8*, 6286–6295. https://doi.org/10.1039/d0tb00471e.

33. Liu, X., Kim, S.-K., and Wang, X. (2016). Thermomechanical liquid crystalline elastomer capillaries with biomimetic peristaltic crawling function. J. Mater. Chem. B *4*, 7293–7302. https://doi.org/10.1039/c6tb02372j.

34. Yang, Y., Zhan, W., Peng, R., He, C., Pang, X., Shi, D., Jiang, T., and Lin, Z. (2015). Graphene-enabled superior and tunable photomechanical actuation in liquid crystalline elastomer nanocomposites. Adv. Mater. *27*, 6376–6381. https://doi.org/10.1002/adma.201503680.

35. Barnes, M., and Verduzco, R. (2019). Direct shape programming of liquid crystal elastomers. Soft Matter *15*, 870–879. https://doi.org/10.1039/c8sm02174k.

36. Jiang, Z., Xiao, Y., and Zhao, Y. (2019). Shining light on liquid crystal polymer networks: preparing, reconfiguring, and driving soft actuators. Adv. Opt. Mater. *7*, 1900262. https://doi.org/10.1002/adom.201900262.

37. Tian, H., Wang, Z., Chen, Y., Shao, J., Gao, T., and Cai, S. (2018). Polydopamine-coated main-chain liquid crystal elastomer as optically driven artificial muscle. ACS Appl. Mater. Interfaces *10*, 8307–8316. https://doi.org/10.1021/acsami.8b00639.

38. Petsch, S., Rix, R., Khatri, B., Schuhladen, S., Müller, P., Zentel, R., Zappe, H., and Physical, A.A. (2015). Smart artificial muscle actuators: liquid crystal elastomers with integrated temperature feedback. Sensor Actuator Phys. *231*, 44–51. https://doi.org/10.1016/j.sna.2014.10.014.

39. Li, M.-H., and Keller, P. (2006). Artificial muscles based on liquid crystal elastomers. Philos. Trans. A Math. Phys. Eng. Sci. *364*, 2763–2777. https://doi.org/10.1098/rsta.2006.1853.

40. He, Q., Wang, Z., Wang, Y., Minori, A., Tolley, M.T., and Cai, S. (2019). Electrically controlled liquid crystal elastomer-based soft tubular actuator with multimodal actuation. Sci. Adv. *5*, eaax5746. https://doi.org/10.1126/sciadv.aax5746.

41. Boothby, J.M., Gagnon, J.C., McDowell, E., Van Volkenburg, T., Currano, L., and Xia, Z. (2022). An untethered soft robot based on liquid crystal elastomers. Soft Robot. *9*, 154–162. https://doi.org/10.1089/soro.2020.0135.

42. Ceamanos, L., Kahveci, Z., López-Valdeolivas, M., Liu, D., Broer, D.J., and Sánchez-Somolinos, C. (2020). Four-dimensional printed liquid crystalline elastomer actuators with fast photoinduced mechanical response towards light-driven robotic functions. ACS Appl. Mater. Interfaces *12*, 44195–44204. https://doi.org/10.1021/acsami.0c13341.

43. Chen, G., Jin, B., Shi, Y., Zhao, Q., Shen, Y., and Xie, T. (2022). Rapidly and repeatedly reprogrammable liquid crystalline elastomer via a shape memory mechanism. Adv. Mater. *34*, e2201679. https://doi.org/10.1002/adma.202201679.

44. Jiang, J., Han, L., Ge, F., Xiao, Y., Cheng, R., Tong, X., and Zhao, Y. (2022). Porous liquid-crystalline networks with hydrogel-like actuation and reconfigurable function. Angew Chem. Int. Ed. Engl. *61*, e202116689. https://doi.org/10.1002/anie.202116689.

45. Ohm, C., Brehmer, M., and Zentel, R. (2010). Liquid crystalline elastomers as actuators and sensors. Adv. Mater. *22*, 3366–3387. https://doi.org/10.1002/adma.200904059.

46. Tokumoto, H., Zhou, H., Takebe, A., Kamitani, K., Kojio, K., Takahara, A., Bhattacharya, K., and Urayama, K. (2021). Probing the in-plane liquid-like behavior of liquid crystal elastomers. Sci. Adv. *7*, eabe9495. https://doi.org/10.1126/sciadv.abe9495.

47. Bai, R., Ocegueda, E., and Bhattacharya, K. (2021). Photochemical-induced phase transitions in photoactive semicrystalline polymers. Phys. Rev. E *103*, 033003. https://doi.org/10.1103/PhysRevE.103.033003.

48. Yakacki, C.M., Saed, M., Nair, D.P., Gong, T., Reed, S.M., and Bowman, C.N. (2015). Tailorable and programmable liquid-crystalline elastomers using a two-stage thiol–acrylate reaction. RSC Adv. *5*, 18997–19001. https://doi.org/10.1039/C5RA01039J.

49. Brömmel, F., Kramer, D., and Finkelmann, H. (2012). Preparation of liquid crystalline elastomers. In Liquid Crystal Elastomers: Materials and Applications (Springer), pp. 1–48. https://doi.org/10.1007/978-3-642-31582-4.

50. Diaz-Calleja, R., and Riande, E. (2012). Biaxially stretched nematic liquid crystalline elastomers. Eur. Phys. J. E Soft Matter *35*, 2. https://doi.org/10.1140/epje/i2012-12002-5.

51. Küpfer, J., and Finkelmann, H. (1991). Nematic liquid single crystal elastomers. Makromol. Chem. Rapid Commun. *12*, 717–726. https://doi.org/10.1002/marc.1991.030121211.

52. Lee, J., Guo, Y., Choi, Y.J., Jung, S., Seol, D., Choi, S., et al. (2020). Mechanically programmed 2D and 3D liquid crystal elastomers at macro-and microscale via two-step photocrosslinking. Soft Matter *16* (11), 2695–2705. https://doi.org/10.1039/C9SM02237F.

53. Jin, B., Liu, J., Shi, Y., Chen, G., Zhao, Q., and Yang, S. (2022). Solvent-assisted 4D programming and reprogramming of liquid crystalline organogels. Adv. Mater. *34*, e2107855. https://doi.org/10.1002/adma.202107855.

54. Luo, C., Chung, C., Yakacki, C.M., Long, K., and Yu, K. (2022). Real-time alignment and

reorientation of polymer chains in liquid crystal elastomers. ACS Appl. Mater. Interfaces *14*, 1961–1972. https://doi.org/10.1021/acsami.1c20082.

55. Agrawal, A., Luchette, P., Palffy-Muhoray, P., Biswal, S.L., Chapman, W.G., and Verduzco, R. (2012). Surface wrinkling in liquid crystal elastomers. Soft Matter *8*, 7138–7142. https://doi.org/10.1039/C2SM25734C.

56. Shin, J., Kang, M., Tsai, T., Leal, C., Braun, P.V., and Cahill, D.G. (2016). Thermally functional liquid crystal networks by magnetic field driven molecular orientation. ACS Macro Lett. *5*, 955–960. https://doi.org/10.1021/acsmacrolett.6b00475.

57. Herbert, K.M., Fowler, H.E., McCracken, J.M., Schlafmann, K.R., Koch, J.A., and White, T.J. (2021). Synthesis and alignment of liquid crystalline elastomers. Nat. Rev. Mater. *7*, 23–38. https://doi.org/10.1038/s41578-021-00359-z.

58. Ambulo, C.P., Burroughs, J.J., Boothby, J.M., Kim, H., Shankar, M.R., and Ware, T.H. (2017). Four-dimensional printing of liquid crystal elastomers. ACS Appl. Mater. Interfaces *9*, 37332–37339. https://doi.org/10.1021/acsami.7b11851.

59. Davidson, E.C., Kotikian, A., Li, S., Aizenberg, J., and Lewis, J.A. (2020). 3D printable and reconfigurable liquid crystal elastomers with light-induced shape memory via dynamic bond exchange. Adv. Mater. *32*, 1905682. https://doi.org/10.1002/adma.201905682.

60. Barnes, M., Sajadi, S.M., Parekh, S., Rahman, M.M., Ajayan, P.M., and Verduzco, R. (2020). Reactive 3D printing of shape-programmable liquid crystal elastomer actuators. ACS Appl. Mater. Interfaces *12*, 28692–28699. https://doi.org/10.1021/acsami.0c07331.

61. Yuan, C., Roach, D.J., Dunn, C.K., Mu, Q., Kuang, X., Yakacki, C.M., et al. (2017). 3D printed reversible shape changing soft actuators assisted by liquid crystal elastomers. Soft Matter *13*, 5558–5568. https://doi.org/10.1039/C7SM00759K.

62. Zhang, C., Lu, X., Fei, G., Wang, Z., Xia, H., and Zhao, Y. (2019). 4D printing of a liquid crystal elastomer with a controllable orientation gradient. ACS Appl. Mater. Interfaces *11*, 44774–44782. https://doi.org/10.1021/acsami.9b18037.

63. Wang, Z., Wang, Z., Zheng, Y., He, Q., Wang, Y., and Cai, S. (2020). Three-dimensional printing of functionally graded liquid crystal elastomer. Sci. Adv. *6*, eabc0034. https://doi.org/10.1126/sciadv.abc0034.

64. Martin Linares, C.P., Traugutt, N.A., Saed, M.O., Martin Linares, A., Yakacki, C.M., and Nguyen, T.D. (2020). The effect of alignment on the rate-dependent behavior of a main-chain liquid crystal elastomer. Soft Matter *16*, 8782–8798. https://doi.org/10.1039/D0SM00125B.

65. Lin, S., Liu, J., Liu, X., and Zhao, X. (2019). Muscle-like fatigue-resistant hydrogels by mechanical training. Proc. Natl. Acad. Sci. USA *116*, 10244–10249. https://doi.org/10.1073/pnas.1903019116.

66. Orrego, S., Chen, Z., Krekora, U., Hou, D., Jeon, S.Y., Pittman, M., Montoya, C., Chen, Y., and Kang, S.H. (2020). Bioinspired materials with self-adaptable mechanical properties. Adv. Mater. *32*, 1906970. https://doi.org/10.1002/adma.201906970.

67. Matsuda, T., Kawakami, R., Namba, R., Nakajima, T., and Gong, J.P. (2019). Mechanoresponsive self-growing hydrogels inspired by muscle training. Science *363*, 504–508. https://doi.org/10.1126/science.aau9533.

68. Wang, Z., Wang, J., Ayarza, J., Steeves, T., Hu, Z., Manna, S., and Esser-Kahn, A.P. (2021). Bio-inspired mechanically adaptive materials through vibration-induced crosslinking. Nat. Mater. *20*, 869–874. https://doi.org/10.1038/s41563-021-00932-5.

69. Alapan, Y., Karacakol, A.C., Guzelhan, S.N., Isik, I., and Sitti, M.J. (2020). Reprogrammable shape morphing of magnetic soft machines. Sci. Adv. *6*, eabc6414. https://doi.org/10.1126/sciadv.abc6414.

70. Tu, Z., Liu, W., Wang, J., Qiu, X., Huang, J., Li, J., and Lou, H. (2021). Biomimetic high performance artificial muscle built on sacrificial coordination network and mechanical training process. Nat. Commun. *12*, 2916–3011. https://doi.org/10.1038/s41467-021-23204-x.

71. Cao, Y., and Hutchinson, J.W. (2012). Wrinkling phenomena in neo-Hookean film/substrate bilayers. J. Appl. Mech. *79*. https://doi.org/10.1115/1.4005960.

72. Hanzon, D.W., Traugutt, N.A., McBride, M.K., Bowman, C.N., Yakacki, C.M., and Yu, K. (2018). Adaptable liquid crystal elastomers with transesterification-based bond exchange reactions. Soft Matter *14*, 951–960. https://doi.org/10.1039/c7sm02110k.

73. Wang, Z., El Hajj Chehade, A., Govindjee, S., and Nguyen, T.D. (2022). A nonlinear viscoelasticity theory for nematic liquid crystal elastomers. J. Mech. Phys. Solid. *163*, 104829. https://doi.org/10.1016/j.jmps.2022.104829.

74. He, X., Zheng, Y., He, Q., and Cai, S. (2020). Uniaxial tension of a nematic elastomer with inclined mesogens. Extreme Mech. Lett. *40*, 100936. https://doi.org/10.1016/j.eml.2020.100936.